Structural and impedance analysis of tin-sulphide (SnS) nanoparticles produced with the help of hydrothermal process

Z. Khan [a], A. D. Khalid [b*], M. I. Khan [c], B. Parveen [a], Ihab M. Moussa [d], M. S. Hassan [e], N.-ur-Rehman [f], A. K. Khan [f], S. Mumtaz [g]
[a] *Department of Physics, Lahore Garrison University, Lahore Pakistan*
[b] *Department of Physics, Superior University, Lahore Pakistan*
[c] *Department of Physics, the University of Lahore, Lahore Pakistan*
[d] *Department of Botany and Microbiology, College of Science, King Saud University, P.O. Box 2455, Riyadh, 11451, Saudi Arabia.*
[e] *Institute of Functional Nano & Soft Materials, (FUNSOM). Soochow University, China*
[f] *The Institute of Physics, The Islamia university of Bahawal pur Pakistan*
[g] *Department of Electrical and Biological Physics, Kwangwoon University, Seoul 01897, South Korea*

The three samples of SnS with different molarity 1ml, 0.5ml and 0.25ml were prepared by hydrothermal method. The prepared samples were characterized by XRD, SEM and impedance spectroscopies. XRD confirmed the cubic and orthorhombic structure of SnS. The average size of nanoparticles was noted to be about 12.77 nm, 16.43 nm and 16.44 nm at 140 °C. These nanoparticles were of cubic and orthorhombic forms. Average strain came out to be 0.215, 0.142 and 0.140. This result shows that by changing molarity, crystal structure of SnS can be changed. Crystallite size is increasing with decreasing molarity while strain is decreasing. Scanning electron microscopy (SEM) was carried out in order to study sheet like morphology of the samples. The carried-out process showed that the produced sample shows ball resembling spherical form. On the other hand, the frequency distribution and calculation of mean size of SnS nanoparticles, histogram and Gaussian curve were drawn and analyzed. Size range of nano-particles for sample 1ml, 0.5ml and 0.25ml was between (10−65) nm, (20−120) nm, (10−90) nm, respectively. The real part of impedance Z' got maximum value of 0.173 MΩ, 0.31 MΩ, and 0.40 MΩ at three different molarities. Maximum values of imaginary impedance observed were 0.053 MΩ (1ml), 0.112 MΩ (0.5ml) and 0.14 MΩ at different Debye relaxation peaks. The results show that reduction in the molarity increases the impedance and decreases the capacitance.

(Received September 10, 2024; Accepted November 18, 2024)

Keywords: SnS, Hydrothermal, Gaussian curve, Impedance, Capacitance

1. Introduction

All through the long haul, semiconductors' nanoparticles are being concentrated on account of a number of factors. Band gap and optical features intensifies their significance. That is why they are having diverse applications. In the range of these properties, SnS nanoparticles are explicitly imperative considering its high maintenance coefficient, and photoelectric change capability besides, it is being used as super capacitor daylight-based cell sensor, photo detector, and photo catalyst. A very demanding nature of SnS is explored in recent past. It is found suitable for producing photovoltaic material [1]. The ingredients required for crystal of SnS are not only in abundance but they are relatively cost effective. Moreover, light transformation effectiveness of 24% is very much interesting and efficient. This value was anticipated for SnS by Loferski. This further makes it significant for photo cells. Moreover, it has shown tremendous scope as a lithium battery anode material and mixture sun-based cells. The values possessed by tin sulphide are

* Corresponding author: ad_khalid82@hotmail.com
https://doi.org/10.15251/CL.2024.2111.933

remarkable. Direct optical band gap (∼1.3 eV) high absorption coefficient in the visible region ($>10^4$ cm^{-1}), carrier mobility of 30 $cm^2V^{-1}s^{-1}$, p-type electrical conductivity [2]. The making elements of SnS are in abundance, nontoxic and cheap. Similarly, the theoretical light conversion efficiency makes them more efficient to be used in photovoltaic cells [3-4]. It is found that SnS has an orthorhombic structure with a = 4.329 Å, b = 11.192 Å, and c = 3.984 Å. It has been observed that band gap energies (E_g) lie in the ranges of 1.049 eV−1.076 eV and a direct band gap of ∼1.3 eV [5]. Such ranges of E_g have suitable SnS uses in devices. This was done when thin films of the said SnS were formed with the help of advanced techniques [6-7]. It was pondered upon in last decade of 20th century. Noguchi et al. [8] worked on it. He was the one who was able to show possibility of n-CdS/p-SnS hetero junction photovoltaic cell. The observed cell had an efficiency of 0.29 percent for conversion. Moreover, there was less importance attached to tin sulphide movement on phenol. Keeping this in mind, photo catalytic productivity was needed to be analyzed. Reuse characteristic of tin sulphide was also needed to be explored using this technique. It was observed by Reddy that such photovoltaic device could have conversion efficiencies of about 1.3 percent [9]. Moreover, a conversion efficiency of 70% was also observed. Conversion efficiency could be made improved up to 2.1 percent from 1.3 percent [10]. There was a continuous improvement underway. It came to a result that it could be improved conversion efficiency of 3.88% was achieved for thermally evaporated SnS absorber and ALD layer of Zn(O,S) [11]. In recent few years, SnS based solar cells ensured considerable advantage and progress and led to efficiency up to 4.36% [12]. In the wake of this, unending efforts have been made to improve performance having control of purity, grain size, grain boundary defects and band gap alignment/engineering. One of the major reasons for this could be the anisotropic physical properties of SnS-ORT [13].

Production of Nano sheets of SnS was required. It was accomplished using the technique of hydrothermal method. As of late, tin sulfide (SnS) has drawn in more considered different specialists stood apart from other gathering small band opening semi-conductors. Its ingredients are bountiful in existence. Gem improvement of SnS embraces the turned NaCl structure that's all there is to it development is easy. [14]. There is a desired value of opening of band for this layer of tin sulphide. This value is in range of 1.3eV and 1eV [15]. SnS has wide range of applications due to its commendable features. They include film sun-based cells, plasma-based depositing of vapors and many more [16] alongside close infrared finders [17]. There are a number of methods employed for successful study of SnS to be used in spray pyro lytic deposition [18], aggregation in the form of vapor [19] and atmospheric pressure CVD [20]. Recent past shows a considerable focus on use of SnS and pertinent research regarding use of nanoparticle nature of tin sulphide. New methods have been used to produce metal chalcogenide semiconductors [21]. Hydrothermal method has been one of the most result-oriented methods for production of Tin sulfide nanostructures [22-26]. Moreover, Nano sheets obtained from it have been synthesized through hydrothermal method in the presence of thioglycolic acid (TGA) and laser ablation method [27-29]. Synthesis of SnS Nano sheets by simple hydrothermal method at calcination temperature 140 °C. The characterization has been done using powder XRD, Scanning electron microscope SEM, Fourier transform infrared (FT-IR) spectroscopy on SnS Nano sheets

2. Synthesis of SnS nanoparticles and characterizations

2.1. Chemicals required

Tin chloride ($SnCl_2$) & Sodium Sulfide (Na_2S) and de-ionized water.

2.2. Synthesis procedure

For the preparation of nanoparticles with different molarities 1 mol, 0.5 mol and 0.25 mol, sodium sulphide (Na_2S) and Tin chloride ($SnCl_2$) were taken in particular proportion as given in Table 1. For preparation of 1 ml SnS, 3.9 g of Na_2S and 9.48 g $SnCl_2$ solutions were prepared separately having 50 ml de-ionized water, it was stirred for a time of 15 minutes until materials mix uniformly. Both solutions were mixed and once again stirred for another 300 seconds. Afterwards, solution of ($SnCl_2$ and Na_2S) was put into autoclave and kept in furnace for 8 hours at

temperature of 140°C. After 8 hours, the autoclave was kept out of furnace and placed to cool down it at room temperature. Then, it was filtered and dried in electric oven for 3 hours at 60°C. The dried precipitates were finely grinded. The similar procedure was repeated for formation of 0.5ml and 0.25ml SnS, by taking amount of $SnCl_2$ and Na_2S as given in Table 1. All materials were then characterized to study their structural and impedance properties.

Table 1. The quantities of precursor materials.

No	Molarity	$SnCl_2$ (gm)	Na_2S (gm)
1	1	9.48	3.9
2	0.5	4.74	1.95
3	0.25	2.37	0.98

2.3. Characterization techniques

Different characterization techniques were applied to study the properties synthesized Nano-particles. X ray diffraction (XRD) method was utilized to study the crystallite size. It was helpful in ascertaining the structure and phase purity of the obtained Nano sheets. Scanning electron microscopy (SEM) was used to study the morphology and shapes of Nano-particles. Impedance analysis was performed to investigate the real and imaginary parts of impedance.

3. Result and discussion

3.1. XRD analysis

This study gave line-scans for SnS and are presented in Figure 1 (a,b,c) with respect to different molarities 1ml, 0.5ml and 0.25ml. Required parameters can be found Using XRD.

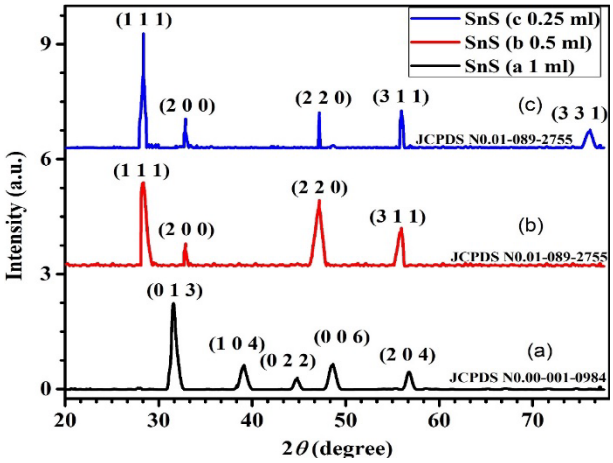

Fig. 1. XRD of SnS at three different molarities.

The peaks identified for 1ml sample (figure1a) showing pure orthorhombic phase of SnS (JCPDS card Reference code: 00-001-0984) having different planes (0 1 3), (1 0 4), (0 2 2), (0 0 6), (2 0 4) at 2θ angles of, 31.5899°, 39.13540°, 44.83090°, 48.6527°, 56.7835°, respectively. While, XRD spectra of 0.5ml showing cubic structure (JCPDS card Reference code: 01-089-2755) with planes (1 1 1), (2 0 0), (2 2 0), (3 1 1), diffracted at 2θ angles of 28.36768°, 32.87170°, 47.173560°, 55.965780°, respectively. Similarly, XRD spectra at 0.25ml also showing cubic SnS (JCPDS card Reference code: 01-089-2755) having different planes (1 1 1), (2 0 0), (2 0 0), (3 1

1), (3 3 1) corresponding to 2θ angles of, 28.36743°, 32.87560°, 47.17300650°, 55.963180°, 76.145741°, respectively.

The cross-section boundaries are determined from the XRD designs, by utilizing relation (1) [30].

$$\frac{1}{d^2} = \frac{h^2}{a^2} + \frac{k^2}{b^2} + \frac{l^2}{c^2} \quad (1)$$

where, (hkl) address Mill operator lists. The sample (a) extricated grid boundaries are exceptionally near the standard upsides of cross section steady, a = 3.9900 A˚, b = 4.3400 A˚ , c = 11.2000 A˚ which are obvious in Table 1. Sample (b) removed grid boundaries are extremely near the standard upsides of cross section steady, a = 5.4450 A˚, b = 5.4450 A˚, c = 5.4450 A˚, as per JCPD reference no. 01-089-2755, as is clear in Table 1. The sample (c) separated grid boundaries are exceptionally near the standard upsides of grid steady, a = 5.4450 A˚, b = 5.4450 A˚, c = 5.4450 A˚, as per JCPD reference no.01-089-2755, as is obvious in Table 1. The diffraction tops expanding is utilized to work out crystallite size. This size of test (a, b, c) is registered from the major (013), (111), (111) tops, the crystallite size of test by utilizing the Debye-Scherer's equation, which is denoted underneath [31].

$$D = \frac{k\lambda}{\beta_{hkl} Cos\theta} \quad (2)$$

In the above relation D is representing size, k denotes shape factor, X-beams frequency and β_{hkl} is the full widths at half maximum that to be calculated in radian. The determined qualities recorded in Table 1. Original tin sulphide possesses a crystallite size 12.77nm, 16.43nm, and 16.44nm. Diminishing the molarity from 1ml to 0.25ml expands the typical crystallite size. The determined upsides of crystallite size show great concurrence with currently founded values. Hasan [32] determined normal crystallite size falling in scope of 5nm to 9nm for Nano-glass like SnS dainty film. Jakhar *et al.* [33] concentrated on the refractive record of SnS thin film and announced normal crystallite size in the scope of 11 to 25 nm. Grid creates strain. Its value is determined with the help of accompanying equation [34]:

$$\varepsilon = \frac{\beta_{hkl}}{4\ tan\theta} \quad (3)$$

The recorded value of strain (Table 1) is found with the help of Wilson condition. This value diminishes from 0.215 to 0.140 when value of molarity goes down form 1ml and reaches 0.25ml. Williamson Lobby (W-H) plot strategy helped in determining required calculation of size and strain utilizing accompanying relation [35]:

$$\frac{\beta_{hkl} Cos\theta}{\lambda} = \frac{4\varepsilon Sin\theta}{\lambda} + \frac{k}{D} \quad (4)$$

In the above relation e addresses strain and size of the crystallite is represented by D. in case of pure form the plotted 4Sinθ/λ along x-hub and βCosθ/λ on y-pivot. Strain is determined from the change of the direct fit lines. Values of size of the crystal and value of strain were determined using Wilson condition and Debye-Scherer's connection, separately, are contrasted and those determined from W-H plots, as introduced in Table 2. An increase in size of crystal was observed for a downward movement of molarity. Separation thickness was calculated with the help $\delta=1/D^2$ [36]. More modest upsides of separation concentration and strain and separation density upgrade free transporter versatility in host grid. Separation thickness alongside strain will quite often diminish with expansion in size. This is indicated in a form of Table 2. A comparative conduct has been seen by Kumar [37]. It was found from X ray diffraction that solitary stage Nano-crystallites might be refined in order to show the necessary arrangement of underlying boundaries, to understand an ideal arrangement of features.

Table 2. Average values of crystal size, strain and dislocation density.

Sr. no.	Molarity (ml)	Average Crystallite size (nm)	Average Strain	Dislocation Density
1	1	12.77	0.215	0.006123
2	0.5	16.43	0.142	0.003702
3	0.25	16.44	0.140	0.003702

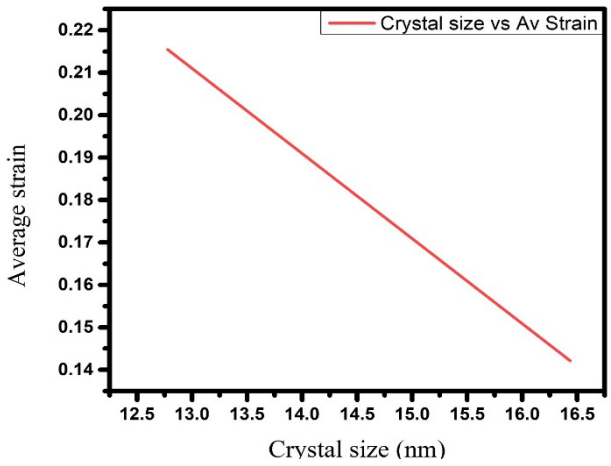

Fig. 2. Average values of crystal size, strain and dislocation density.

All XRD spectra are showing pure phase at every molarity either pure orthorhombic or cubic. These result shows in Figure (2) that by changing molarity crystal structure of SnS can be changed. Crystallite size is increasing with decreasing molarity while strain is decreasing.

3.2. Surface morphology

The surface morphology was studied by the application of scanning electron microscopy (SEM images). It resulted in the observation of details that were magnified and enlarged. The results of three samples having different molarities are shown in Figure 2, describe the shape of SnS nanoparticles. For frequency distribution, mean particle size calculation of Tin Sulphide nanoparticles, histogram in addition to Gaussian curve were drawn and analyzed.

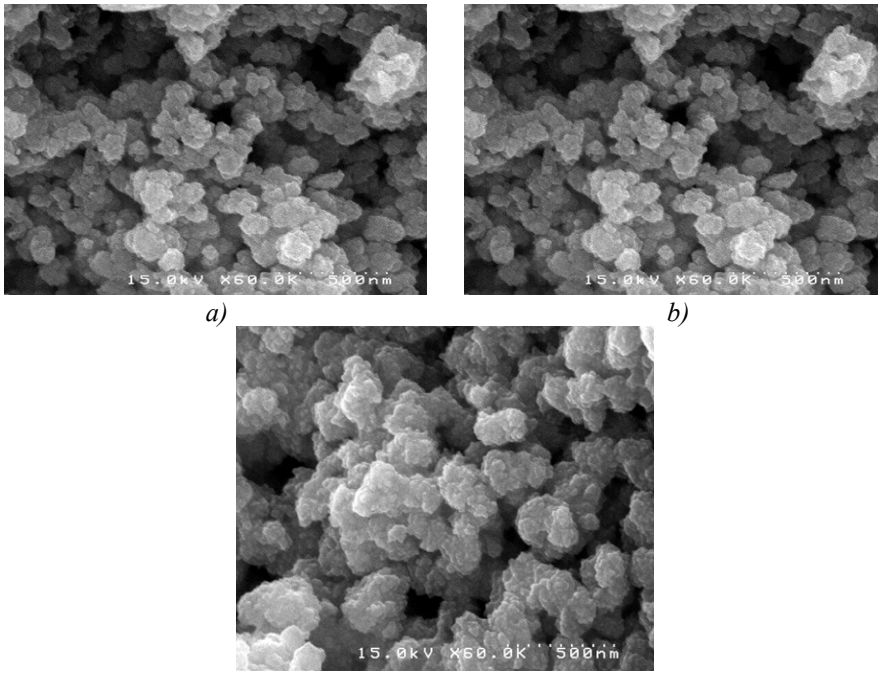

a) *b)* *c)*

Fig. 3. (a,b,c): SEM of SnS at three different molarities.

Image J software was used to analyze particle size and to plot histogram. Particle size of almost 100 particles was calculated which were used to draw the histogram and Gaussian cure. On the other hand, it is made evident by the frequency distribution that for how diverse value set appears. The representation in the form of Guass distribution would delineate probable. This distribution is somehow symmetric around an average value. The Figure 3 (a, b, c) is showing SEM images at different molarities and Figure 4 (a, b, c) are the histograms of size distribution of nanoparticles. All samples are confirming the nanoparticles and denser distribution of grains. Furthermore, the agglomeration is increasing with decreasing molarity.

Size range of Nano-particles is between 10nm to 65nm for 1ml sample, as given in Figure 2b. Maximum particles are present in (20–25) nm and (30− 35) nm region. Average size of nanoparticles is 27nm. While for 0.5ml sample, size range of Nano-particle is 20 nm to 120 nm. Maximum particles are present in (50−60) nm region and average size observed is 49nm. With further decrease in molarity, size range of Nano-particles observed is 10 nm to 90 nm and maximum particles are present in (20−30) nm region with average size 32 nm.

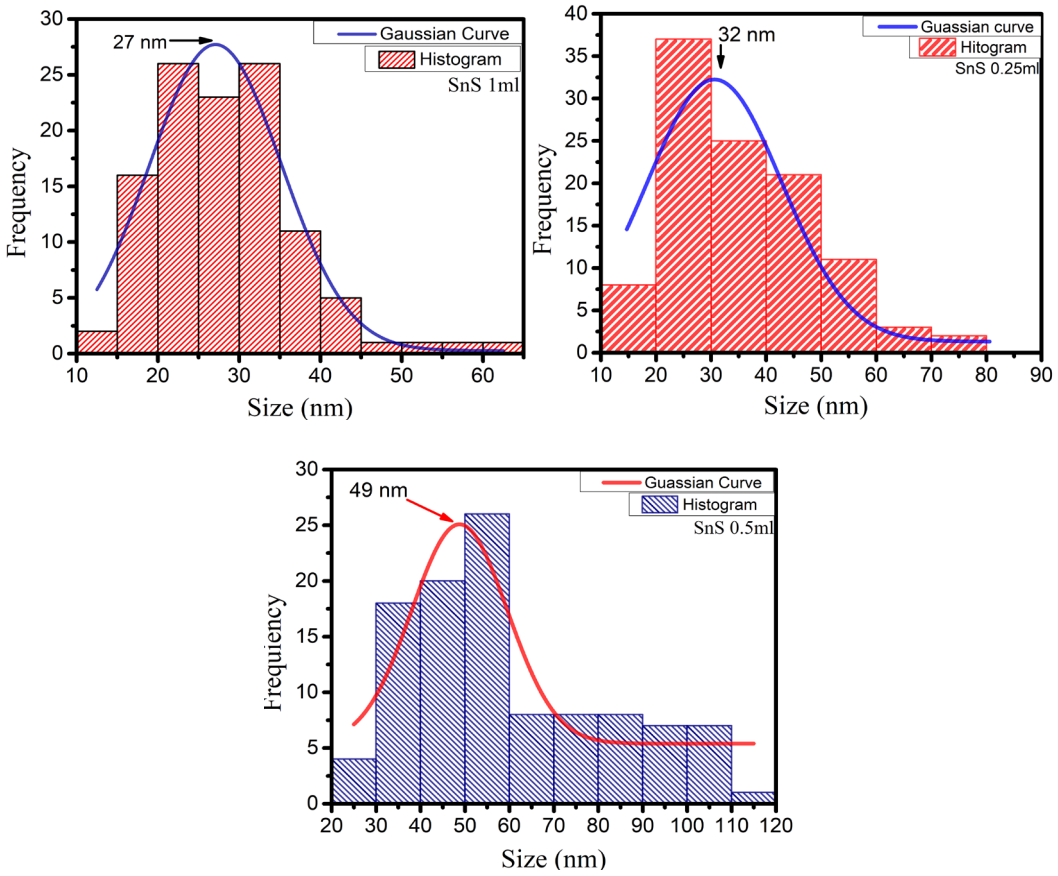

Fig. 4. Grain size determined from SEM at three different molarities.

3.3. Impedance analysis

Impedance spectroscopy was performed to study the impedance of samples at various molarities. Calculated values of impedance are drawn in diagram 5-6 against incident value of frequency. Figure 5 is representing variation of real component of impedance (Z') with frequency. The real part of impedance Z' gets on enhancing with increasing frequency and gets maximum value of 0.173 MΩ, 0.31 MΩ, and 0.40 MΩ at three different molarities. While with further increase in frequency, the value of impedance falls. Moreover, complex impedance spectroscopy is used for studying the behavior of tin sulphide particles. The obtained information reveals useful information about capacitive nature alongside resistive attribute. These features are studied in the complicated plain that is because of crescents arrangement. These half circles address electrical attribute was displayed by grains, their boundaries alongside in case of points of interaction. Z* could be addressed regarding real Z' and unreal Z'' portions in case of impedance [38]:

$$Z^* = Z' + iZ'' = R + \frac{i}{\omega C} \tag{5}$$

The real and imaginary values of impedance are shown for frequency in Figures 5 and 6. Figure 5 addresses variety of real part of impedance (Z') with frequency. The real piece of impedance (Z') gets on upgrading with expanding recurrence and gets most extreme worth of 0.173 MΩ, 0.31 MΩ, and 0.40 MΩ at three distinct molarities. While with additional expansion in frequency, the calculated value of impedance decreases.

Figure 5 demonstrates frequency-based varieties noticed in case of real part of impedance. It becomes evident to show that Z' goes upgraded when value of frequency goes down. It decreases when additional rise in frequency is observed, after which it came to be consistent, and a comparative conduct has been noticed for tests. The abatement in Z' at larger value of frequency may be because of the greater ac conductivity.

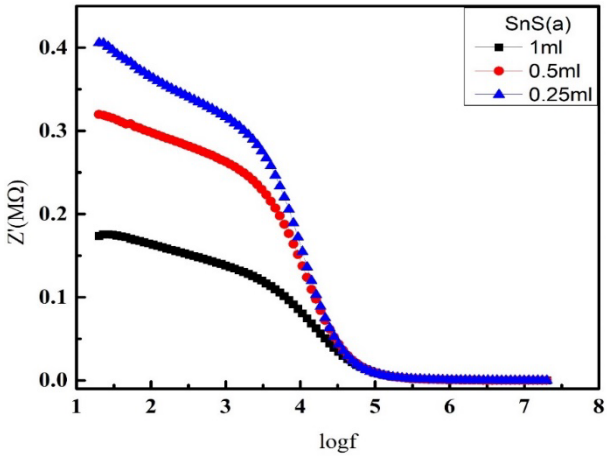

Fig. 5. Real Impedance (Z') of SnS at three different molarities.

The imaginary part of impedance Z" is shown in Figure 6. All graphs are showing relaxation peaks at different impedance values. Maximum value of imaginary impedance observed were 0.053 MΩ (1ml), 0.112 MΩ (0.5ml) and 0.14 MΩ at different Debye relaxation peaks.

Figure 6 addresses imaginary impedance Z" drawn against falling frequency. It is obvious from figure that Z" indicates tops, arrives at a greatest and afterward diminishes with additional expansion in frequency. Imaginary piece of impedance Z" is displayed in Figure 6.

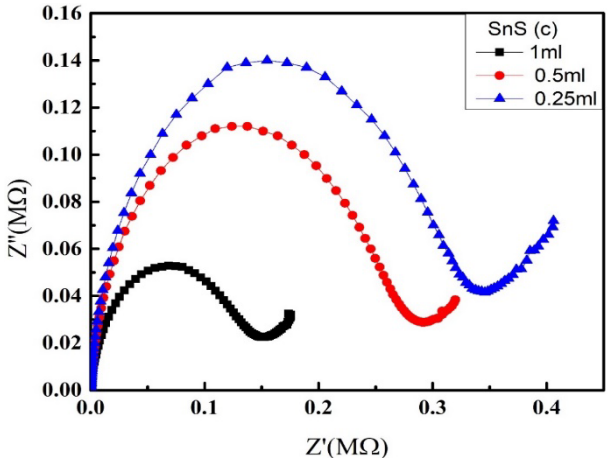

Fig. 6. Imaginary Impedance (Z") of SnS at three different molarities.

All diagrams are showing unwinding peak at various values of impedance. Larger value of impedance noticed were 0.053 MΩ (1ml), 0.112 MΩ (0.5ml) and 0.14 MΩ at various Debye unwinding peak.

Imaginary impedance versus real impedance values were also plotted (Figure 7) to study grains resistance and grains capacitance. Nyquist plots clearly describe details related to grain and their boundaries. The plot makes it very much clear by explaining the formation of a half circle in case of all samples. This half circle represents conduction of grains. Similarly, the other semicircle lies at the very beginning and hence in a shape of a straight line. An ideal form of half circle that possesses its center at real z axis denotes Debye relaxation. So, drawn Figurer's were helpful in finding out values of grain resistance and grain capacitance. It is represented by Rg & C_g. The value of Rg & C_g which are listed in Table 3.

Debye peak is seen for falling frequency becomes equivalent for a frequency termed as electronic bouncing frequency. Attributes pertinent to electrical nature in case of unadulterated SnS tests are obvious because of the half circle circular segments arrangement. Graphical representation done for Z'' and Z' were given the name as Nyquist plots. These plots were shown having Figure 4c. For most part, the grains and calculated pertinent grain limits were employable in case of varying frequency [39]. quite obvious in Figure that there seems one-half circle for every one of the examples, addressing the grain limit conduction, while the subsequent half circle is right toward the beginning and consequently show up as a straight line. An ideal half circle having focus at genuine Z-hub uncovers a Debye ideal curve. In given diagrams, we determined obstruction Rg, capacitance Cg and time required for relaxation denoted by tg, these were additionally introduced having Table 3. Introduced value might communicate a comparable circuit framed by the determined upsides of the resistance and the capacitance [40].

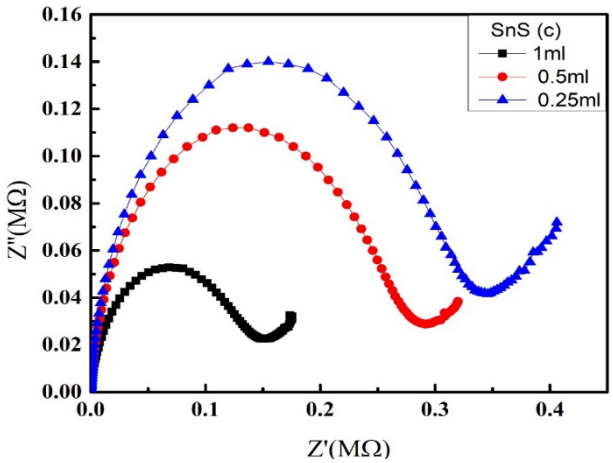

Fig. 7. Nyquist Graph Z' & Z'' of SnS at three different molarities.

Table 3. The grain resistance and grain capacitance.

Sample no.	Sample (ml)	Grain-resistance R_g (MΩ)	Grain-capacitance C_g (nF)
1	1	0.17152	0.136
2	0.5	0.31363	0.065
3	0.25	0.39551	0.052

4. Conclusion

For the first time Nano sheets were synthesized by hydrothermal method at 140°C calcination temperature. XRD analysis confirm that SnS Nano sheets have orthorhombic structure for 1ml as molarity changes the SnS Nano sheets transfer to cubic structure. Scanning electron microscopy found that Nano sheets were formed. SEM images are showing spherical type nature. The grains are not uniformly spread all over the surface. The grain size increases with changing the molarity. Impedance analyzer indicates the frequency-dependent variations. Z' goes on increasing with respect to small incident values of frequency. If value of frequency is further increased Imaginary impedance Z'' reaches to a maximum value, obtains a peak and finally diminishes with further rise in incident value of frequency. For samples 1ml, 0.5ml and 0.25ml of different molarities have maximum impedance values are 0.053 MΩ, 0.112 MΩ and 0.14 MΩ, respectively at same frequency 4.14 HZ. These results show that reduction in the molarity increases the real impedance with respect to imaginary impedance. Graphical representation of two

values of impedance i.e Z" and Z' is called Nyquist plot. Moreover, Debye relaxation is obtained in case of Z' at center.

Funding: Researchers supporting project number (RSPD2024R741), King Saud University.

Acknowledgement

The authors would like to thank the Researchers Supporting Project number (RSPD2024R741), King Saud University, Riyadh, Saudi Arabia.

References

[1] Tariq, Ghulam Hasnain, Ghulam Asghar, M. Shahzad Shifa, M. Anis-Ur-Rehman, Physical Chemistry Chemical Physics 25, no. 46 (2023): 31726-31740; https://doi.org/10.1039/D3CP04332K

[2] Messaoudi, Meriem, Leila Lamiri, Samah Boudour, Lynda Beddek, Optical and Quantum Electronics 56, no. 8 (2024): 1375; https://doi.org/10.1007/s11082-024-07216-7

[3] Tumram, Priya V., Renuka Nafdey, Pranay R. Kautkar, Materials Science and Engineering: B 307 (2024): 117504; https://doi.org/10.1016/j.mseb.2024.117504

[4] Li, Yang, Shisheng Zheng, Hao Liu, Nature Communications 15, no. 1 (2024): 176; https://doi.org/10.1038/s41467-023-44131-z

[5] Hegde, S. S., Prashantha Murahari, Brian Jeevan Fernandes, Journal of Alloys and Compounds 820 (2020): 153116; https://doi.org/10.1016/j.jallcom.2019.153116

[6] I. Y. Ahmet, M. Guc, Y. Sánchez, M. Neuschitzer, V. Izquierdo-Roca, E. Saucedo, A. L. Johnson, RSC Adv., 9 (2019) 14899-14909; https://doi.org/10.1039/C9RA01938C

[7] M. Devika, N. K. Reddy, M. Prashantha, K. Ramesh, S. V. Reddy, Y. B. Hahn, K. R. Gunasekhar, Phys. Status Solidi A, 207 (2010) 1864-1869; https://doi.org/10.1002/pssa.200925379

[8] Voznyi, Andrii, Volodymyr Kosyak, Yurii Yeromenko, Thin Solid Films 709 (2020): 138153; https://doi.org/10.1016/j.tsf.2020.138153

[9] Iguchi, Yuki, Koichi Sato, Kazutoshi Inoue, Solid State Sciences 140 (2023): 107206; https://doi.org/10.1016/j.solidstatesciences.2023.107206

[10] T. Ikuno, R. Suzuki, K. Kitazumi, N. Takahashi, N. Kato, K. Higuchi, Appl. Phys. Lett., 102 (2013) 193901; https://doi.org/10.1063/1.4804603

[11] V. Steinmann, R. Jaramillo, K. Hartman, R. Chakraborty, R. E. Brandt, J. R. Poindexter, Y. S. Lee, L. Sun, A. Polizzotti, H. H. Park, R. G. Gordon, T. Buonassisi, Adv. Mater., 26 (2014) 7488-7492; https://doi.org/10.1002/adma.201402219

[12] P. Sinsermsuksakul, L. Sun, S. W. Lee, H. H. Park, S. B. Kim, C. Yang, R. G. Gordon, Adv. Energy Mater., 4 (2014) 1400496; https://doi.org/10.1002/aenm.201400496

[13] J. A. Andrade-Arvizu, M. Courel-Piedrahita, O. Vigil-Galán, J. Mater. Sci. Mater. Electron., 26 (2015) 4541-4556; https://doi.org/10.1007/s10854-015-3050-z

[14] Banotra, Arun, Naresh Padha. Journal of Crystal Growth 534 (2020): 125460; https://doi.org/10.1016/j.jcrysgro.2019.125460

[15] Ichimura M, Takeuchi K, Ono Y, Arai E. Thin Solid Films 2000;98:361-8; https://doi.org/10.1016/S0040-6090(99)00798-1

[16] Sebastian, S., I. Kulandaisamy, S. Valanarasu, Mohd Shkir, V. Ganesh, I. S. Yahia, Hyun-Seok Kim, Dhanasekaran Vikraman, Surface Engineering 37, no. 2 (2021): 137-147; https://doi.org/10.1080/02670844.2020.1754623

[17] Pramanik P, Basu PK, Biswas S. Thin Solid Films 1987;150:269-76; https://doi.org/10.1016/0040-6090(87)90099-X

[18] Thangaraju B, Kaliannan P. J Phys D Appl Phys 2000;33:1054-9; https://doi.org/10.1088/0022-3727/33/9/304

[19] Ortiz A, Alonso JC, Garcia M, Toriz J. Semicond Sci Technol 1996;11:243-7; https://doi.org/10.1088/0268-1242/11/2/017

[20] Price LS, Parkin IP, Hardy AME, Clark RJH, Hibbert TG, Molloy KC. Chem Mater 1999;11:1792-9; https://doi.org/10.1021/cm990005z

[21] Xiao ZL, Han CY, Kwok WK, Wang HH, Welp U, Wang J, et al. J Am Chem Soc 2004;126:2316-7; https://doi.org/10.1021/ja0315154

[22] Zhu H, Yang D, Zhang H. Mater Lett 2006;60:2686-9; https://doi.org/10.1016/j.matlet.2006.01.065

[23] Panda SK, Gorai S, Chaudhuri S. Mater Sci Eng B 2006;129:265-9; https://doi.org/10.1016/j.mseb.2005.12.014

[24] Peng H, Jiang L, Huang J, Li G. J Nanopart Res 2007;9:1163-5; https://doi.org/10.1007/s11051-006-9208-0

[25] Liu Y, Hou D, Wang G. Chem Phys Lett 2003;379:67-73; https://doi.org/10.1016/j.cplett.2003.08.014

[26] Chen D, Shen G, Tang K, Lei S, Zheng H, Qian Y. J Cryst Growth 2004;260:469-74; https://doi.org/10.1016/j.jcrysgro.2003.09.009

[27] Zhu H, Yang D, Ji Y, Zhang H, Shen XJ. Mater Sci 2005;40:591-5; https://doi.org/10.1007/s10853-005-6293-x

[28] Salavati- Niasari M, Ghanbari D, Davar F. J Alloy Comp 2010;492:570-5; https://doi.org/10.1016/j.jallcom.2009.11.183

[29] Kang JG, Ko YD, Choi KJ, Park JG, Kim DW. Appl Phys A 2010.

[30] Reghima M, Akkari A, Guasch C, Turki-Kamoun N (2015), J Appl Phys 7:023128; https://doi.org/10.1063/1.4918740

[31] Cullity B (1967) Elements of X-ray diffraction. AddisionWesley publishing company Inc, New york, p 501

[32] Kuznetsov AY, Machado R, Gomes LS, Achete CA, Swamy V, Muddle BC, Prakapenka V (2009), Appl Phys Lett 94:193117; https://doi.org/10.1063/1.3139078

[33] Hasan BA, Shallal IH (2014), J Nano Adv Mater 2:43-49; https://doi.org/10.12785/jnam/020201

[34] Jakhar A, Jamdagni A, Bakshi A, Verma T, Shukla V (2013), Solid State Commun 168:31-35; https://doi.org/10.1016/j.ssc.2013.06.013

[35] Manohari AG, Dhanapandian S, Manoharan C, Kumar KS, Maralinga T (2014), Mater Sci Semicond Process 17:138-142; https://doi.org/10.1016/j.mssp.2013.09.012

[36] Ahmad SM, Latif LA, Salim AK (2011), J Basrah Res Sci 37:54-59

[37] Guneri E, Gode F, Ulutas C, Kirmizigul F, Altindemir G (2010), Chalcogenide Lett 7:685-694

[38] Kumar KS, Manoharan C, Dhanapandian S, Manohari AG (2013), Mol Biol Spectrosc 115:840-844; https://doi.org/10.1016/j.saa.2013.06.112

[39] Jayasree J, Chalapathi U, Raja VS (2013), Thin Solid Films 537:149-155; https://doi.org/10.1016/j.tsf.2013.03.013

[40] Azam A, Ahmed AS, Ansari MS, Shafeeq M, Naqvi AH (2010), J Alloys Compd 506:237-242; https://doi.org/10.1016/j.jallcom.2010.06.184